AGU ADVANCING EARTH AND SPACE SCIENCES

Geophysical Research Letters

RESEARCH LETTER
10.1029/2023GL106980

The Chemical Effect of Increased Water Vapor From the Hunga Tonga-Hunga Ha'apai Eruption on the Antarctic Ozone Hole

Ingo Wohltmann[1], Michelle L. Santee[2], Gloria L. Manney[3,4], and Luis F. Millán[2]

[1]Alfred Wegener Institute, Helmholtz Centre for Polar and Marine Research, Potsdam, Germany, [2]Jet Propulsion Laboratory, California Institute of Technology, Pasadena, CA, USA, [3]NorthWest Research Associates, Socorro, NM, USA, [4]New Mexico Institute of Mining and Technology, Socorro, NM, USA

Key Points:

- The Hunga Tonga-Hunga Ha'apai eruption increased water vapor in the emerging Antarctic vortex in 2023 by 20%–40% compared to earlier years
- The increased water vapor from Hunga Tonga had a minor effect on Antarctic ozone depletion through the end of October (less than 4 DU)
- This minor effect is due to low, but not unusual, vortex temperatures that reset water vapor anomalies before they could impact ozone loss

Correspondence to:
I. Wohltmann,
ingo.wohltmann@awi.de

Citation:
Wohltmann, I., Santee, M. L., Manney, G. L., & Millán, L. F. (2024). The chemical effect of increased water vapor from the Hunga Tonga-Hunga Ha'apai eruption on the Antarctic ozone hole. *Geophysical Research Letters*, *51*, e2023GL106980. https://doi.org/10.1029/2023GL106980

Received 24 OCT 2023
Accepted 31 JAN 2024

Author Contribution:
Conceptualization: Ingo Wohltmann
Methodology: Ingo Wohltmann
Software: Ingo Wohltmann
Writing – original draft: Ingo Wohltmann

Abstract The eruption of the Hunga Tonga-Hunga Ha'apai volcano on 15 January 2022 was one of the most explosive eruptions of the last decades. The amount of water vapor injected into the stratosphere was unprecedented in the observational record, increasing the stratospheric water vapor burden by about 10%. Using model runs from the ATLAS chemistry and transport model and Microwave Limb Sounder (MLS) satellite observations, we show that while 20%–40% more water vapor than usual was entrained into the Antarctic polar vortex in 2023 as it formed, the direct chemical effect of the increased water vapor on Antarctic ozone depletion in June through October was minor (less than 4 DU). This is because low temperatures in the vortex, as occur every year in the Antarctic, limit water vapor to the saturation pressure and thus reset any anomalies through the process of dehydration before they can affect ozone loss.

Plain Language Summary The eruption of the Hunga Tonga-Hunga Ha'apai volcano on 15 January 2022 was one of the most explosive eruptions of the last decades. An amount of water vapor unprecedented in the observational record was injected into the stratosphere, increasing the total stratospheric water vapor mass by about 10%. Using model runs and satellite observations, we show that while the dispersion of the plume increased water vapor in the Antarctic in 2023 by 20%–40% at the beginning of the ozone hole season compared to earlier years, the effect of the increased water vapor on the Antarctic ozone hole was minor. This is because low temperatures in the vortex, as occur every year in the Antarctic, limit water vapor due to condensation and thus reset any anomalies before they can affect ozone loss.

1. Introduction

The eruption of the Hunga Tonga-Hunga Ha'apai volcano on 15 January 2022 was one of the most violent eruptions of the last decades. It reached a volcanic explosivity index (VEI) of 5, and the plume reached an altitude of more than 50 km (e.g., Carr et al., 2022; Millán et al., 2022; Proud et al., 2022; Schoeberl et al., 2022). An amount of water vapor unprecedented in the observational record was injected into the stratosphere, increasing the stratospheric water vapor burden by about 10% or 150 Tg (Millán et al., 2022; Schoeberl et al., 2022; Vömel et al., 2022). While the increased water vapor was not able to penetrate into the 2022 Antarctic vortex (Manney et al., 2023), the dispersion of the plume increased water vapor observed by MLS in the developing Antarctic vortex in 2023 by about 20%–40% compared to earlier years (in the pressure range of 56.2–17.7 hPa or approximate altitude range 20–28 km).

Here and in the following, the vortex is defined as the volume inside the −36 PVU contour (1 PVU = 10^{-6} K m^2 kg^{-1} s^{-1}) of modified potential vorticity (which scales potential vorticity to have a similar range of values throughout the stratosphere) calculated from a reference level of θ_0 = 475 K (Lait, 1994). This definition results in the vortex edge at 475 K potential temperature in August and September lying near −58° equivalent latitude.

Figure 1(a) shows vortex-averaged profiles of MLS measurements of water vapor (version 5, Livesey et al., 2022) in the developing Antarctic vortex for all years of the MLS record (2005–2023) on 20 May. Typical water vapor profiles at the end of May in the years before 2023 are very similar. In comparison, the profile of 2023 shows increased values throughout a large vertical range. For example, values at 21.5 km increased from an average 4.6 ppm in earlier years to 6.7 ppm in 2023.

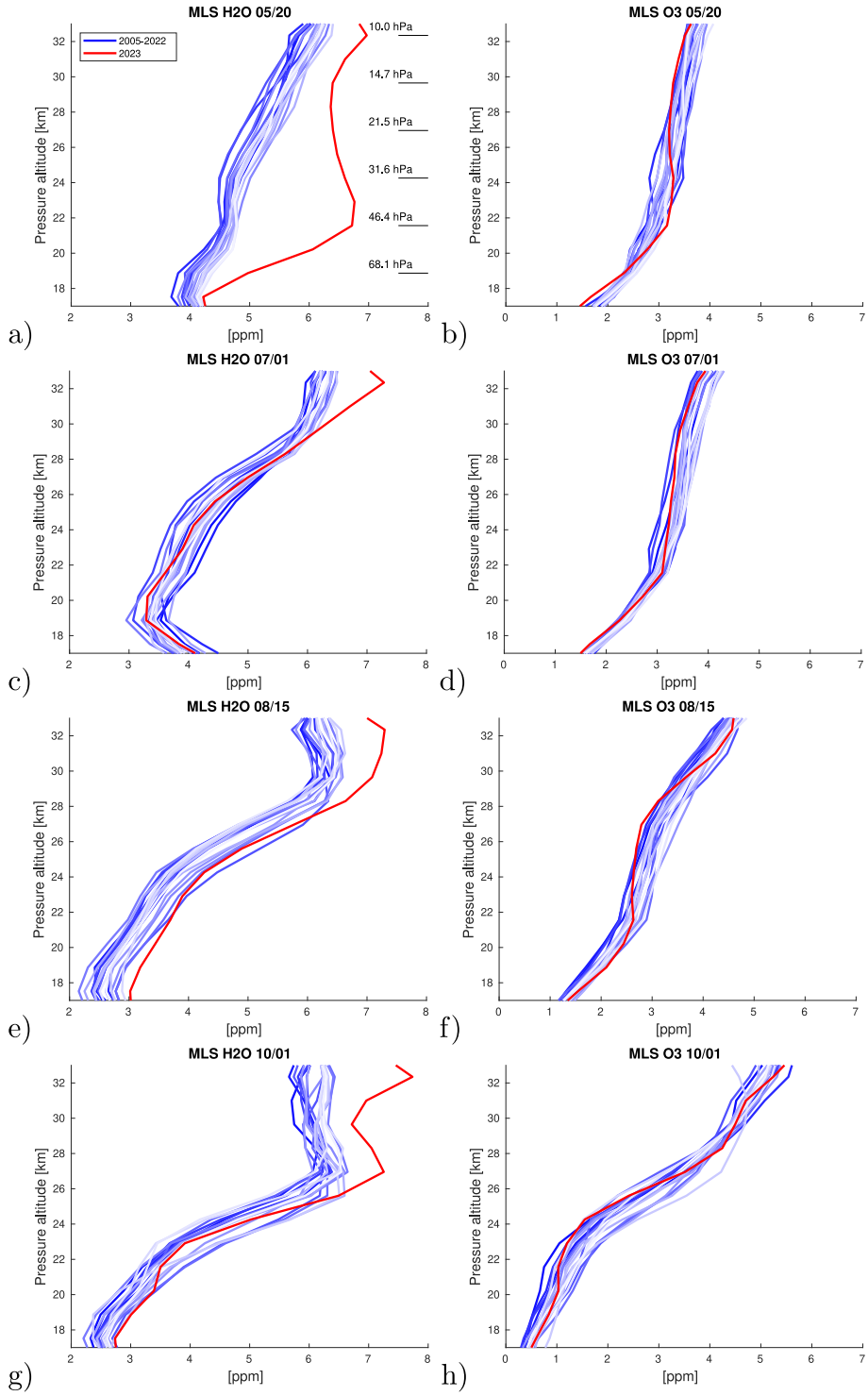

Figure 1. Left: Vortex-averaged water vapor profiles observed by MLS on 20 May (a), 1 July (c), 15 August (e) and 1 October (g) for all years of the MLS data record. 2005–2022 in shades of blue, 2023 is highlighted in red. Right: Same for ozone (b, d, f, h). Profiles are averaged over all MLS measurements of the given day inside the −36 PVU contour of modified potential vorticity. Every other MLS pressure level is indicated in panel (a).

It was speculated that the increased water vapor from the eruption could lead to increased ozone depletion in the Antarctic ozone hole in 2023 (e.g., Manney et al., 2023; Millán et al., 2022). Water vapor can influence polar ozone depletion mainly by its effect on polar stratospheric clouds (PSCs), for example, by changes in formation temperature thresholds, particle size distribution, or dehydration and denitrification. However, MLS measurements in September and October 2023 show that ozone values are not exceptional and are well within the range of earlier years. This can be seen in Figure 1(h), which shows vortex-averaged profiles of MLS measurements of ozone on 1 October after the end of the most severe ozone loss period.

However, it is not possible to attribute interannual changes in ozone to changes in water vapor based on measurements alone. Interannual differences in temperature, transport, or the amount of ozone-depleting substances (ODSs) can have a significant effect on the interannual variability.

In addition to the effect on PSCs, changes in water vapor also cause changes in radiation, and in turn dynamical changes that could affect ozone (e.g., Schoeberl et al., 2022; Wang et al., 2023). However, we concentrate on the chemical changes in this study.

2. Model Setup

We perform runs of the global ATLAS chemistry and transport model (CTM) (Wohltmann et al., 2010; Wohltmann & Rex, 2009) to disentangle the effects of water vapor and other factors such as temperature on ozone. A reference run is initialized with the MLS data from 1 May 2023. A sensitivity run uses exactly the same setup, with the exception of the initialization of MLS water vapor, which is taken from the preceding year on 1 May 2022 (i.e., without the effect of Hunga Tonga on water vapor).

Since a CTM and not a CCM (chemistry-climate model) is used, radiative and dynamical feedbacks are not simulated. Meteorological variables like temperature are required to be the same in the reference and sensitivity run to isolate the effects of differences in water vapor arising from differences in PSC formation and their consequent effects on ozone loss.

The model setup is almost the same as that in Wohltmann et al. (2021), and we refer the reader to that paper for more details. Model runs are driven by meteorological data from the European Centre for Medium-Range Weather Forecasts (ECMWF) ERA5 reanalysis (provided on a $1.125° \times 1.125°$ horizontal grid, 3 hr temporal resolution, and 137 model levels) (Hersbach et al., 2017, 2020). The ATLAS model horizontal resolution is 150 km. The vertical range of the model domain is 13–50 km (about 350–1900 K potential temperature). The model was run from 1 April 2023 to 31 October 2023. Chemical species are initialized on 1 May after a 1-month spin-up period for transport and mixing; chemistry is only simulated after 1 May. O_3, H_2O, HCl, N_2O, HNO_3, and CO are initialized from all MLS measurements on 1 May for the reference run. The other chemical species are initialized from climatologies as described in Wohltmann et al. (2021).

While we refer to the model description papers for most details of the PSC parameterization, the parameterization of dehydration is important for our study. Dehydration is modeled in a deliberately simple fashion in ATLAS, which is justified by the good agreement of water vapor with observations (many of these validation results have not been published, but Figure 21 and 22 of Wohltmann et al. (2017) show two examples). Above a given supersaturation, all water vapor is removed from the model instantaneously (i.e., there is no sedimentation to lower levels). For this study and earlier studies, we use a value for supersaturation of 0.7 (corresponding to a supercooling of about 3 K below the freezing point). The value was empirically adjusted to fit the water vapor measurements in earlier studies. The impact on the vortex-averaged water vapor compared to a run that assumes no supersaturation is about 0.5 ppm at 475 K potential temperature (not shown).

3. Results

Most of the following figures show the time evolution of vortex-averaged mixing ratios of different species in the reference run, the sensitivity run, and in the MLS data at 475 K potential temperature. It is not possible in these plots to show exactly the same air masses over the course of time because of processes such as mixing and differential descent in the vortex. Hence, the temporal change seen in the figures is always the sum of both dynamical and chemical changes. We use the 475 K level for illustrative purposes and have carefully considered dynamical effects where it is necessary (e.g., when calculating chemical ozone loss).

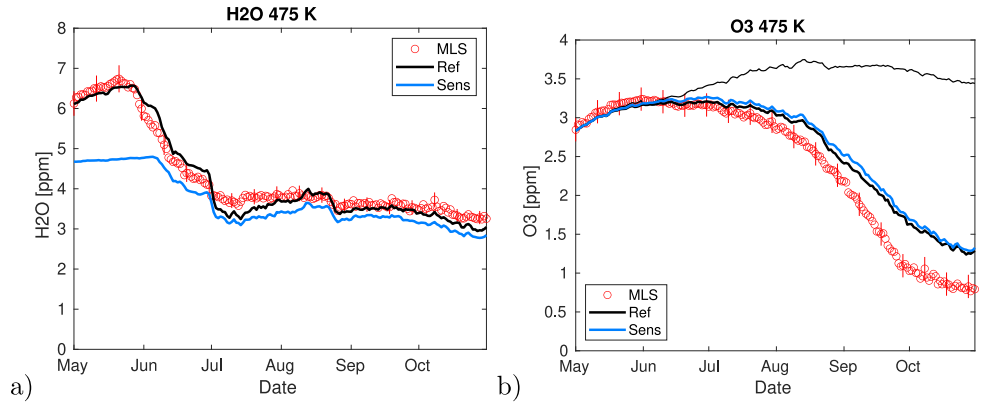

Figure 2. Left (a): Vortex-averaged water vapor at 475 K potential temperature observed by MLS in 2023 (red dots) and modeled by ATLAS (blue and black lines). The black line shows the reference run initialized with MLS measurements from 2023, while the blue line shows the sensitivity run initialized with MLS water vapor data from 2022 (i.e., without the effect of Hunga Tonga on water vapor). Right (b): Same for ozone. The thin black line shows a passive ozone tracer initialized on 1 June. The difference between the thin black line and the other lines quantifies the amount of ozone loss.

Figure 2(a) shows the time evolution of vortex-averaged water vapor in the reference run, the sensitivity run, and in the MLS data at 475 K potential temperature. The reference run and MLS show excellent agreement over the complete time period. Water vapor starts with values of about 6–7 ppm in May, but quickly decreases to values of about 3–4 ppm between mid-May and the start of July. This decrease is caused by dehydration, which limits water vapor to the saturation pressure through condensation and sedimentation in the very cold polar vortex. The decrease is also visible in the MLS profiles in Figures 1c, 1e and 1g, except at the highest altitudes where water vapor does not exceed the saturation limit. Figures 1c, 1e and 1g also show that water vapor is well within the range of previous years by the beginning of July.

MLS can only observe water vapor (gas-phase H_2O); it does not see ice condensed in cloud particles, and thus it does not measure total H_2O. We account for this by comparing the observations only to the simulated gas-phase H_2O from ATLAS. The fraction of the total H_2O condensed in clouds is negligible for most time periods of the model run, but it reaches 50% or more for individual model air parcels during the intervals of most intense dehydration and sequestration in June and July. However, the vortex average of the H_2O condensed in clouds is negligible compared to the gas-phase H_2O. That means that the change seen in Figure 2a is mainly caused by dehydration and not by sequestration.

In addition, we checked the supersaturation of water vapor over ice based on individual MLS observations and ECMWF temperatures. These calculations show that supersaturations of up to 0.3 are routinely observed by MLS. This relies on an accurate representation of the temperatures in ECMWF. Small uncertainties in the temperatures can easily cause large changes in interpretation, since the saturation pressure is very sensitive to temperature.

Figure 2(a) shows that the sensitivity run starts at values below 5 ppm that do not agree well with the measurements (as expected). However, the sensitivity run quickly converges to the reference run by early July (differences are less than 0.4 ppm after early July). This is because in both cases the temperatures are sufficiently low that water vapor abundances are mostly above the saturation limit. Once the saturation limit is reached, water vapor in both runs is equalized.

Vortex temperatures in 2023 were close to the long-term mean and not exceptionally low (see e.g. NASA GSFC, 2023). Temperatures low enough to cause widespread dehydration are a common feature of all Antarctic winters in the observational record. Hence, no unusual meteorological situtation is needed to explain the reset of water vapor in 2023.

Figure 2(b) shows the corresponding time evolution of vortex-averaged ozone at 475 K. The difference between the reference run and the sensitivity run is very small throughout the whole time period. This is because ozone loss initiated by heterogeneous activation of chlorine and bromine is only significant within the sunlit portion of the vortex from July through September. The thin black line shows a passive ozone tracer initialized on 1 June. The

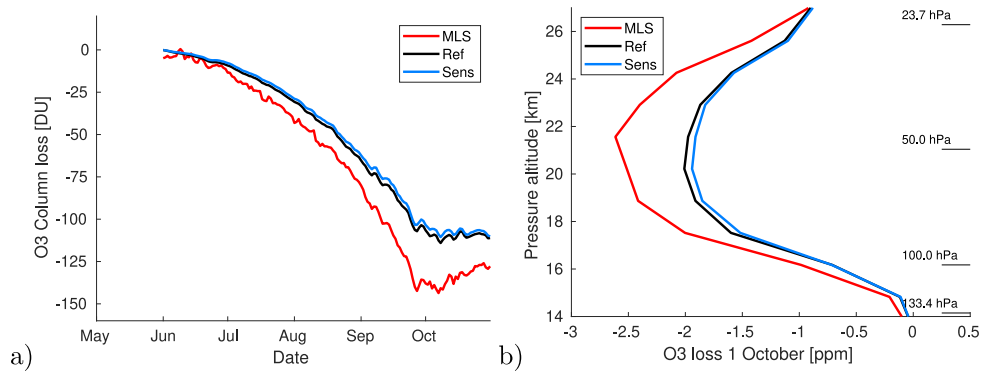

Figure 3. Left (a): Vortex-averaged chemical loss of ozone modeled by ATLAS for the partial column from 133.4 to 23.7 hPa. Ozone loss was determined by subtracting a passive ozone tracer initialized on 1 June from the modeled ozone values. The black line shows the reference run initialized with MLS measurements from 2023, while the blue line shows the sensitivity run initialized with MLS water vapor data from 2022 (i.e., without the effect of Hunga Tonga on water vapor). The red line shows ozone loss determined by subtracting the passive ozone tracer from the ozone values observed by MLS (based on the MLS retrieval levels from 121.2 to 26.1 hPa and the integration limits from above). Right (b): Corresponding vortex-averaged chemical ozone loss profiles on 1 October.

difference between the passive ozone tracer and the other lines quantifies the amount of ozone loss. There is only a short time period before July (cf. Figure 2(a)) when differences in water vapor between the runs can affect ozone loss.

The difference between the modeled ozone and the passive ozone tracer underestimates ozone loss by about 0.7 ppm (30%) compared to the difference between the passive ozone tracer and MLS ozone. Since ATLAS runs for other Antarctic winters agree better with MLS (e.g., in Wohltmann et al., 2021, Fig. 9, ozone loss in October agrees within 10% for 2006 and 2011), this discrepancy might hint that other effects from the Hunga Tonga eruption are occurring. However, as outlined before, it cannot be the direct effect of water vapor. Since the radiative and dynamical effects of Hunga Tonga are probably at least partly captured in the ECMWF data, the SO_2 injection by the eruption and ensuing changes in stratospheric aerosol could play a role here.

ClO mixing ratios measured by MLS typically agree within 10% with the ClO mixing ratios modeled by ATLAS in the reference run (not shown). This indicates that the chlorine activation in the model compares well with observations, suggesting that the discrepancy is not caused by an underestimation of chlorine activation.

The results at other potential temperature levels lead to similar conclusions, and the effect of the increased water vapor remains small throughout the ozone column. Figure 3(a) shows the chemical ozone loss modeled by ATLAS for the partial column from 133.4 to 23.7 hPa. Figure 3 (b) shows the corresponding vortex-averaged chemical ozone loss profiles on 1 October. Ozone loss was determined by subtracting the passive ozone tracer initialized on 1 June from the modeled or MLS ozone values. Since the value of the passive ozone tracer is not known for air masses that entered through the upper model boundary after 1 June and descended in the vortex, the column is restricted to 23.7 hPa. The figure shows that the effect of the increased water vapor on the column loss in the model is small (less than 4 DU) and that ATLAS consistently underestimates ozone loss compared to MLS in most of the pressure range.

4. Discussion and Summary

There are several ways in which water vapor might change ozone loss in addition to dehydration.

- The threshold temperatures for the formation of all PSC types (supercooled ternary solution (STS), nitric acid trihydrate (NAT) and ice) are increased by the increased water vapor. For example, a change in water vapor from 5 to 6 ppm increases the threshold temperature for ice by 1.1 K at 50 hPa (Marti & Mauersberger, 1993), and for NAT by 0.8 K (for a HNO_3 mixing ratio of 10 ppb) (Hanson & Mauersberger, 1988). STS has no defined threshold temperature for formation but shows a gradual increase of reaction rates and droplet volume with lower temperatures. However, an increase in water vapor from 5 to 6 ppm has to a good approximation

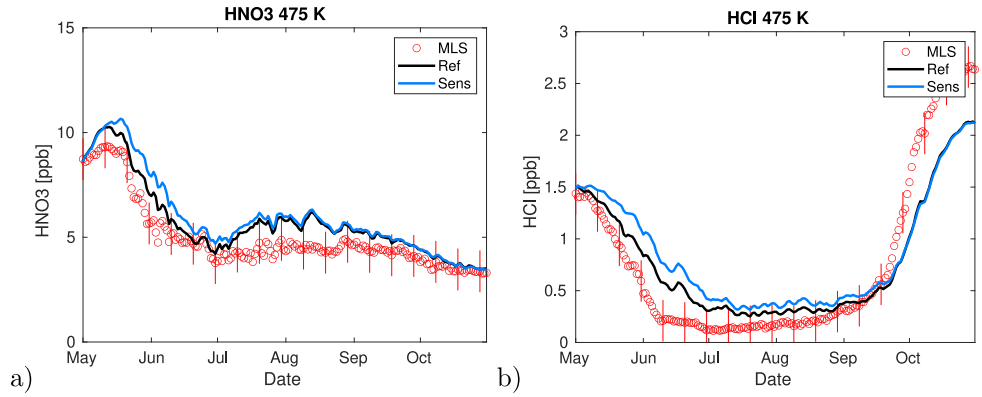

Figure 4. Left (a): Vortex-averaged HNO_3 (gas phase) at 475 K potential temperature observed by MLS in 2023 (red dots) and modeled by ATLAS (blue and black lines). The black line shows the reference run initialized with MLS measurements from 2023, while the blue line shows the sensitivity run initialized with MLS water vapor data from 2022 (i.e., without the effect of Hunga Tonga on water vapor). Right (b): Same for HCl (gas phase).

the same effect on the STS reactivity (time needed for the HCl + $ClONO_2$ reaction to completely deplete one of the reaction partners) as a temperature change of 1 K (Carslaw et al., 1995; Hanson & Ravishankara, 1994) (for 2 ppb HCl, 1 ppb $ClONO_2$, 0.15 ppb H_2SO_4, number density of droplets 10 cm^{-3}).

While these changes increase the volume inside the vortex where the formation of PSCs is possible, this can only have an effect before dehydration sets in. The effects of changes in threshold temperatures and STS reactivity are included in ATLAS. Figure 2(b) shows that they have no large effect on ozone depletion.

- Changes in water vapor have an effect on the particle size distribution of all cloud types. There is more water vapor available above the saturation limit, and one might expect larger particle sizes and larger surface area densities. However, particle formation and growth is a complex process, and this might not be straightforward. As in many chemistry and transport models, PSCs are treated in a somewhat simplified manner in ATLAS (Tritscher et al., 2021). For NAT and ice clouds, a constant number density is assumed, and a uniform particle size is then calculated from the HNO_3 and H_2O available above the saturation pressure. That is, the uniform particle size will simply increase in our model. For STS, a constant number density and a log-normal distribution is assumed that is scaled with the total liquid volume.

  Figure 2(b) shows very small differences in ozone between the reference and sensitivity runs, implying that the effect of changes in particle size distribution must have been small. However, particle growth and formation might be more complex in reality and the effect on ozone depletion may be larger. Changes in size distribution may also have an effect after dehydration sets in (i.e., differences in the size distribution of NAT, ice and STS PSCs caused by increased water vapor in May and June might be persistent or lead to changes in the size distribution in later months).
- Since larger particles have a greater fall velocity, dehydration might also be faster in 2023. However, this is not considered in the simple ATLAS dehydration parameterization. The good agreement between ATLAS and MLS suggests that dehydration might be a fast enough process so that the speed of the process does not matter for the amount of ozone depletion.
- Denitrification might also be affected by differences in the formation of the NAT particles. Denitrification is treated in a more sophisticated manner than dehydration in ATLAS and incorporates the nucleation, growth, sedimentation, and evaporation of individual particles with the DLAPSE model (Davies et al., 2005). Figure 4(a) shows that the changes in gas-phase HNO_3 (which are mainly caused by denitrification) are small between the reference run and the sensitivity run. The amount of HNO_3 taken up in the clouds and not visible in the MLS measurements is generally small compared to the gas-phase HNO_3 mixing ratios and the effects of denitrification, see for example, Figure 2 of Wohltmann et al. (2017).

Figure 4(b) shows vortex-averaged gas-phase HCl at 475 K for MLS and ATLAS. Unfortunately, there are issues that prevent drawing any firm conclusions (including the amount of activation) from comparison of gas-phase HCl observed by MLS with the model results. It is a well-known deficiency of most CTMs (not only ATLAS) that there is a marked discrepancy between measured and modeled HCl mixing ratios in the Antarctic vortex (e.g.,

Brakebusch et al., 2013; Grooß et al., 2018; Solomon et al., 2015; Wohltmann et al., 2017). This points to a lack of understanding of the chemical and microphysical processes determining HCl in the Antarctic vortex. The ATLAS model runs include an empirical correction to improve the agreement between measurements and model based on one of the possible reasons for the discrepancy (HCl solubility), see the description of the model setup in Wohltmann et al. (2021). One issue that is important for winter 2023 in particular is that the solubility of HCl in STS droplets is a very strong function of water vapor. This is the cause of the differences in gas-phase HCl between the reference and sensitivity run.

In summary, we have shown that while the Hunga Tonga-Hunga Ha'apai eruption increased water vapor in the emerging Southern Hemisphere stratospheric polar vortex by 20–40% in 2023, ozone values at the end of September in the Antarctic ozone hole were in no way exceptional and were well within in the range of earlier years. ATLAS model runs indicate that the chemical and microphysical effect of the increased water vapor on Antarctic ozone depletion was minor (less than 4 DU difference in column loss in September and October). The reason for this are the very low climatological temperatures in the vortex, which limit water vapor to the saturation pressure in any year of the observational record and tend to reset any anomalies in water vapor through dehydration before they can affect ozone loss. However, the ATLAS runs underestimate observed ozone loss in 2023 by about 30% (in contrast to good agreement with observations within 10% in similar studies for other winters). Further studies are needed to understand the causes of this discrepancy and whether it may be related to other effects from the Hunga Tonga-Huga Ha'apai eruption in addition to the increased water vapor and dehydration, such as changes in SO_2.

Data Availability Statement

ATLAS source code is available at Wohltmann (2023). Aura MLS Level 2 data are available at Schwartz et al. (2020), Lambert et al. (2020), Manney et al. (2020) and Froidevaux et al. (2020). ECMWF ERA5 data are available at Hersbach et al. (2017).

Acknowledgments
ECMWF ERA5 and ERA5T data (Hersbach et al., 2017) was downloaded from the Copernicus Climate Change Service (C3S) (2023). The results contain modified Copernicus Climate Change Service information 2023. Neither the European Commission nor ECMWF is responsible for any use that may be made of the Copernicus information or data it contains. Work at the Jet Propulsion Laboratory, California Institute of Technology, was carried out under a contract with the National Aeronautics and Space Administration (80NM0018D0004). G. L. Manney was supported by the Jet Propulsion Laboratory (JPL) Microwave Limb Sounder team under JPL subcontract #1521127 to NWRA. We thank Peter von der Gathen for helpful comments and discussion. Open Access funding enabled and organized by Projekt DEAL.

References

Brakebusch, M., Randall, C. E., Kinnison, D. E., Tilmes, S., Santee, M. L., & Manney, G. L. (2013). Evaluation of whole atmosphere community climate model simulations of ozone during Arctic winter 2004–2005. *Journal of Geophysical Research: Atmospheres*, *118*(6), 2673–2688. https://doi.org/10.1002/jgrd.50226

Carr, J. L., Horváth, Á., Wu, D. L., & Friberg, M. D. (2022). Stereo plume height and motion retrievals for the record-setting Hunga Tonga-Hunga Ha'apai eruption of 15 January 2022. *Geophysical Research Letters*, *49*(9). https://doi.org/10.1029/2022GL098131

Carslaw, K. S., Clegg, S. L., & Brimblecombe, P. (1995). A thermodynamic model of the system HCl-HNO3-H2SO4-H2O, including solubilities of HBr, from < 200 to 328 K. *Journal of Physical Chemistry*, *99*(29), 11557–11574. https://doi.org/10.1021/j100029a039

Davies, S., Mann, G. W., Carslaw, K. S., Chipperfield, M. P., Kettleborough, J. A., Santee, M. L., et al. (2005). 3-D microphysical model studies of Arctic denitrification: Comparison with observations. *Atmospheric Chemistry and Physics*, *5*(11), 3093–3109. https://doi.org/10.5194/acp-5-3093-2005

Froidevaux, L., Livesey, N., & Read, W. (2020). MLS/Aura level 2 hydrogen chloride (HCl) mixing ratio V005 [Dataset]. Goddard Earth Sciences Data and Information Services Center (GES DISC). Accessed: 09/2023–12/2023. https://doi.org/10.5067/Aura/MLS/DATA2509

Grooß, J.-U., Müller, R., Spang, R., Tritscher, I., Wegner, T., Chipperfield, M. P., et al. (2018). On the discrepancy of HCl processing in the core of the wintertime polar vortices. *Atmospheric Chemistry and Physics*, *18*(12), 8647–8666. https://doi.org/10.5194/acp-18-8647-2018

Hanson, D., & Mauersberger, K. (1988). Laboratory studies of the nitric acid trihydrate: Implications for the south polar stratosphere. *Geophysical Research Letters*, *15*(8), 855–858. https://doi.org/10.1029/GL015i008p00855

Hanson, D. R., & Ravishankara, A. R. (1994). Reactive uptake of ClONO2 onto sulfuric acid due to reaction with HCl and H2O. *Journal of Physical Chemistry*, *98*(22), 5728–5735. https://doi.org/10.1021/j100073a026

Hersbach, H., Bell, B., Berrisford, P., Hirahara, S., Horányi, A., Muñoz-Sabater, J., et al. (2020). The ERA5 global reanalysis. *Quarterly Journal of the Royal Meteorological Society*, *146*(730), 1999–2049. https://doi.org/10.1002/qj.3803

Hersbach, H., Bell, B., Berrisford, P., Hirahara, S., Horányi, A., Muñoz-Sabater, J., & Thépaut, J.-N. (2017). Complete ERA5 from 1940: Fifth generation of ECMWF atmospheric reanalyses of the global climate [Dataset]. Copernicus Climate Change Service (C3S) Data Store (CDS). Accessed 2023. https://doi.org/10.24381/cds.143582cf

Lait, L. R. (1994). An alternative form for potential vorticity. *Journal of the Atmospheric Sciences*, *51*(12), 1754–1759. https://doi.org/10.1175/1520-0469(1994)051<1754:aaffpv>2.0.co;2

Lambert, A., Read, W., & Livesey, N. (2020). MLS/Aura level 2 water vapor (H2O) mixing ratio V005 [Dataset]. Goddard Earth Sciences Data and Information Services Center (GES DISC). Accessed: 09/2023–12/2023). https://doi.org/10.5067/Aura/MLS/DATA2508

Livesey, N. J., Read, W. G., Wagner, P. A., Froidevaux, L., Santee, M. L., Schwartz, M. J., & Lay, R. R. (2022). Earth observing system (EOS) aura Microwave Limb sounder (MLS) version 5.0x level 2 and 3 data quality and description document. *JPL D-105336 Rev. B*.

Manney, G., Santee, M., Froidevaux, L., Livesey, N., & Read, W. (2020). MLS/Aura level 2 nitric acid (HNO3) mixing ratio V005 [Dataset]. Goddard Earth Sciences Data and Information Services Center (GES DISC). Accessed: 09/2023–12/2023). https://doi.org/10.5067/Aura/MLS/DATA2511

Manney, G. L., Santee, M. L., Lambert, A., Millán, L. F., Minschwaner, K., Werner, F., et al. (2023). Siege in the southern stratosphere: Hunga Tonga-Hunga Ha'apai water vapor excluded from the 2022 Antarctic polar vortex. *Geophysical Research Letters*, *50*(14). https://doi.org/10.1029/2023GL103855

Marti, J., & Mauersberger, K. (1993). A survey and new measurements of ice vapor pressure at temperatures between 170 and 250 K. *Geophysical Research Letters*, *20*(5), 363–366. https://doi.org/10.1029/93GL00105

Millán, L., Santee, M. L., Lambert, A., Livesey, N. J., Werner, F., Schwartz, M. J., et al. (2022). The Hunga Tonga-Hunga Ha'apai hydration of the stratosphere. *Geophysical Research Letters*, *49*(13). https://doi.org/10.1029/2022GL099381

NASA GSFC. (2023). National Aeronautics and Space administration goddard Space flight center (NASA GSFC) annual meteorological statistics. (Accessed 12/2023). Retrieved from https://acd-ext.gsfc.nasa.gov/Data_services/met/ann_data.html

Proud, S. R., Prata, A. T., & Schmauß, S. (2022). The January 2022 eruption of Hunga Tonga-Hunga Ha'apai volcano reached the mesosphere. *Science*, *378*(6619), 554–557. https://doi.org/10.1126/science.abo407

Schoeberl, M. R., Wang, Y., Ueyama, R., Taha, G., Jensen, E., & Yu, W. (2022). Analysis and impact of the Hunga Tonga-Hunga Ha'apai stratospheric water vapor plume. *Geophysical Research Letters*, *49*(20). https://doi.org/10.1029/2022GL100248

Schwartz, M., Froidevaux, L., Livesey, N., & Read, W. (2020). MLS/Aura level 2 ozone (O3) mixing ratio V005 [Dataset]. Goddard Earth Sciences Data and Information Services Center (GES DISC). Accessed: 09/2023–12/2023). https://doi.org/10.5067/Aura/MLS/DATA2516

Solomon, S., Kinnison, D., Bandoro, J., & Garcia, R. (2015). Simulation of polar ozone depletion: An update. *Journal of Geophysical Research: Atmospheres*, *120*(15), 7958–7974. https://doi.org/10.1002/2015JD023365

Tritscher, I., Pitts, M. C., Poole, L. R., Alexander, S. P., Cairo, F., Chipperfield, M. P., et al. (2021). Polar stratospheric clouds: Satellite observations, processes, and role in ozone depletion. *Reviews of Geophysics*, *59*(2). https://doi.org/10.1029/2020RG000702

Vömel, H., Evan, S., & Tully, M. (2022). Water vapor injection into the stratosphere by Hunga Tonga-Hunga Ha'apai. *Science*, *377*(6613), 1444–1447. https://doi.org/10.1126/science.abq2299

Wang, X., Randel, W., Zhu, Y., Tilmes, S., Starr, J., Yu, W., et al. (2023). Stratospheric climate anomalies and ozone loss caused by the Hunga Tonga-Hunga Ha'apai volcanic eruption. *Journal of Geophysical Research: Atmospheres*, *128*(22). https://doi.org/10.1029/2023JD039480

Wohltmann, I. (2023). Snapshot of the source code of the ATLAS model for the manuscript "The chemical effect of increased water vapor from the Hunga Tonga-Hunga Ha'apai eruption on the Antarctic ozone hole" [Software]. Zenodo. https://doi.org/10.5281/zenodo.10391159

Wohltmann, I., Lehmann, R., & Rex, M. (2010). The Lagrangian chemistry and transport model ATLAS: Simulation and validation of stratospheric chemistry and ozone loss in the winter 1999/2000. *Geoscientific Model Development*, *3*(2), 585–601. https://doi.org/10.5194/gmd-3-585-2010

Wohltmann, I., Lehmann, R., & Rex, M. (2017). A quantitative analysis of the reactions involved in stratospheric ozone depletion in the polar vortex core. *Atmospheric Chemistry and Physics*, *17*, 10535–10563. https://doi.org/10.5194/acp-17-10535-2017

Wohltmann, I., & Rex, M. (2009). The Lagrangian chemistry and transport model ATLAS: Validation of advective transport and mixing. *Geoscientific Model Development*, *2*, 153–173. https://doi.org/10.5194/gmd-2-153-2009

Wohltmann, I., von der Gathen, P., Lehmann, R., Deckelmann, H., Manney, G. L., Davies, J., et al. (2021). Chemical evolution of the exceptional Arctic stratospheric winter 2019/2020 compared to previous Arctic and Antarctic winters. *Journal of Geophysical Research: Atmospheres*, *126*(18). https://doi.org/10.1029/2020JD034356